LIMNOLOGY and OCEANOGRAPHY

ASLO

Limnol. Oceanogr. 65, 2020, 191–203

doi: 10.1002/lno.11291

Saharan dust deposition initiates successional patterns among marine microbes in the Western Atlantic

Trace Borchardt,[1,†] Kelsey V. Fisher,[2,†] Alina M. Ebling,[3] Jason R. Westrich,[4] Peng Xian,[5] Christopher D. Holmes,[3] William M. Landing,[3] Erin K. Lipp,[4] Michael S. Wetz,[6] Elizabeth A. Ottesen[1*]

[1]Department of Microbiology, University of Georgia, Athens, Georgia
[2]Department of Life Sciences, Texas A&M University-Corpus Christi, Corpus Christi, Texas
[3]Department of Earth, Ocean, and Atmospheric Science, Florida State University, Tallahassee, Florida
[4]Department of Environmental Health Science, University of Georgia, Athens, Georgia
[5]United States Naval Research Laboratory, Washington, District of Columbia
[6]Harte Research Institute for Gulf of Mexico Studies, Texas A&M University-Corpus Christi, Corpus Christi, Texas

Abstract

Deposition of aerosolized desert dust can affect marine microbial community structure and function through pulsed addition of limiting micro- and macronutrients. However, few studies have captured responses to dust deposition in situ following trans-oceanic transport. We conducted a 26-d time series evaluating biogeochemical and microbial community response to Saharan dust deposition in surface waters in the subtropical western Atlantic (Florida Keys National Marine Sanctuary, U.S.A.). Following periods of elevated atmospheric dust concentrations, particulate and dissolved iron concentrations increased in surface waters. Autotrophic picoeukaryote abundance increased rapidly, followed by increases in the abundance of heterotrophic bacteria and *Synechococcus*. Concomitant to cell count changes, we observed successional shifts in bacterial community composition. The relative abundances of *Prochlorococcus* and *Pelagibacter* declined with dust arrival, while relative abundance of heterotrophic bacteria increased, beginning with Vibrionales and followed sequentially by Chrysophyceae, Rhodobacteriaceae, and Flavobacteriaceae. Finally, a peak in *Synechococcus* cyanobacteria was observed. These results provide new insight into microbial community succession in response to Saharan dust deposition, their association with temporal dynamics in surface water dissolved and particulate iron concentrations, and a potential role for bioprocessing of dust particles in shaping marine microbial responses to deposition events.

Dusts from the earth's deserts are mobilized into the atmosphere where they are transported as aerosols across the globe and eventually deposited. In downwind marine systems, dust deposition can affect the structure and function of marine microbial communities (Mills et al. 2004; Duarte et al. 2006; Davey et al. 2008; Pulido-Villena et al. 2008, 2014; Hill et al. 2010; Laghdass et al. 2011; Langlois et al. 2012; Guieu et al. 2014). Particulate dust or dust leachate has been shown to provide nutrients, particularly iron, nitrate, phosphorus, or a combination thereof, to marine surface waters (Mills et al. 2004; Davey et al. 2008; Langlois et al. 2012; Wuttig et al. 2013; Westrich et al. 2016). Consequently, the temporary relief of nutrient limitation via dust can lead to blooms of specific taxa (e.g., *Vibrio* and *Trichodesmium*) (Lenes et al. 2001; Rahav et al. 2016; Westrich et al. 2016, 2018) or changes in functional processes such as nitrogen fixation (Lenes et al. 2001; Mills et al. 2004; Davey et al. 2008; Rahav et al. 2016). Responses in the autotrophic and heterotrophic microbial populations are observable within a few hours of dust addition, but the responses of specific groups vary depending on the source of dust, length of atmospheric transport, and initial conditions in the seawater (e.g., Hill et al. 2010; Laghdass et al. 2011; Guo et al. 2016). In general, evidence shows that dust addition can stimulate both heterotrophic and autotrophic communities for some period of time before returning to baseline conditions (e.g., Lekunberri et al. 2010; Marín et al. 2017; Pitta et al. 2017*b*). These shifts can have significant effects on carbon cycling, by causing the trophic state to shift from net autotrophy to net heterotrophy (Astrahan et al. 2016; Tsiaras et al. 2017).

Our understanding of microbial responses to dust events has been greatly expanded by experimental studies. However, interpretation of results of experimental manipulations is complicated by the potential for "bottle effects," or incubation-driven

*Correspondence: ottesen@uga.edu

Additional Supporting Information may be found in the online version of this article.

[†]These authors contributed equally to this work.

alterations in microbial community responses (Lee and Fuhrman 1991; Massana et al. 2001). Furthermore, accurately replicating a dust deposition event is difficult, as dust undergoes substantial chemical and physical modification during atmospheric transport (Mahowald et al. 2005, 2018; Baker and Croot 2010). While experimental studies have gone to significant effort to simulate these modifications (Guieu et al. 2010), it is difficult to gauge the effectiveness of these manipulations in the absence of field studies for comparison.

Recent work has described important community responses to dust events in the Mediterranean, which receives high levels of deposition from nearby sources (Pitta et al. 2017*a*). However, much less is known about microbial responses in areas far downwind of desert sources. These areas receive dust that has been highly processed during atmospheric transport, which can significantly affect the bioavailability of associated trace metals and nutrients compared to aerosols with shorter transport time in the atmosphere (Moxim et al. 2011). The objective of this work was to determine how natural Saharan dust aerosols reaching western subtropical North Atlantic surface waters alter microbial population dynamics and community composition. We expected that dust deposition would be associated with an increase in iron concentrations in surface waters, and potentially with increases in nitrogen, and phosphorus. While previous studies have focused on the phytoplankton response to dust amendments, less attention has been placed on the role of early responders, such as heterotrophic bacteria, that may be important in processing dust-associated trace metals and nutrients. We have previously shown that populations of culturable *Vibrio* spp. increase significantly within 14–24 h of dust deposition (Westrich et al. 2016), but less is known about the change in community structure. Based on our prior research, we hypothesized that the early in situ response to dust would be in the form of rapid growth by opportunistic heterotrophic bacteria, accompanied or perhaps followed by an increase in autotrophic microbes. Together, we expected these results to provide improved understanding of microbial community succession in response to atmospheric dust deposition.

Materials and methods

Time series study area and metadata

A time series station was established at Looe Key Reef in the Florida Keys Marine Sanctuary (24°32′41.42″N, 81°24′33.098″W). Seawater samples for trace metals, nutrients, dissolved organic carbon (DOC), total dissolved nitrogen (TDN), chlorophyll *a* (Chl *a*), cell counts, and microbial community analysis were collected once per day (between 14:00 and 18:30 h UTC) at < 0.5 m depth for a 26-d period (12 July 2016 through 06 August 2016). No samples were collected on 17–21 July or on 02 August due to adverse weather conditions. For microbial community analysis, samples were collected in sterile polypropylene bottles. For total and dissolved iron (Fe), nutrients, DOC, TDN, Chl *a*, and cell counts, seawater samples were collected in acid-washed bottles using appropriate measures to avoid trace metal contamination during collection (e.g., Bruland et al. 1979). All samples were stored in the dark on ice until return to shore (~ 1 h) for processing.

Salinity was measured every 20 min with a DS5X multiparameter Sonde (Hach) attached to a mooring at about 2 m depth. Temperature was measured every hour with a HOBO temperature logger (Onset) sited similarly. Total and dust-specific aerosol optical thickness (AOT) were tracked using satellite products available through NASA (https://worldview.earthdata.nasa.gov/) and the aerosol reanalysis product from Naval Research Laboratory (NRL)-Navy Aerosol Analysis and Prediction System (NAAPS) (www.nrlmry.navy.mil/aerosol/) (Westphal et al. 2009; Lynch et al. 2016). Daily rainfall accumulation over the study area was estimated using NOAA's NCEP Environmental Modeling Center (EMC) Stage IV quantitative precipitation estimate (Lin 2011).

Aerosol samples, integrated over 24 h, were collected at ground level (~ 1 m, to estimate surface deposition) at an ocean-facing location on Big Pine Key, FL, U.S.A. (24°38′4.16″N, 81°21′17.02″W, ~ 10 km from the offshore station) with a high-volume aerosol sampler (model 5170-VBL, Tisch Environmental), which pulls air at approximately 1.2 m^3 min^{-1} through 12 replicate acid-washed 47 mm nitrocellulose filter disks (Whatman 41). Aerosol sample collection began on 15 July and ended on 06 August. Rainwater events were collected on Cudjoe Key, FL, U.S.A. (24°39′07.2″N, 81°28′34.2″W) with an acid-washed polycarbonate funnel attached to an acid-washed polyethylene receiving bottle.

Analysis of dissolved and particulate Fe, nutrients, dissolved organic matter, and Chl *a*

All handling and processing of samples for trace element analysis (subsampling, filtration, etc.) was performed in a Class-100 HEPA laminar flow hood at the Mote Marine Lab Center for Tropical Research. For Fe concentrations, seawater and rainwater samples were vacuum-filtered through acid-washed 47 mm 0.2 μm pore size polycarbonate track-etched (PCTE) membrane filters. The filtrate was acidified with 6 mol L^{-1} quartz-distilled (qd) HCl to a final concentration of 0.024 mol L^{-1} HCl and the filters were then frozen until analysis. Filtrates were processed for dissolved Fe (dFe) by the Mg-Fe coprecipitation isotope dilution method described in Saito and Schneider (2006). Samples were analyzed using the Thermo Scientific Element 2 (E2) HR-ICP-MS and dFe concentrations were calculated using a standard isotope dilution equation. Particulate Fe in seawater was determined by digesting the PCTE filters using a microwave digestion method with concentrated (15.8 mol L^{-1}) qd HNO_3 and 28 mol L^{-1} HF (*Optima*) as described in Ebling and Landing (2015). Fe concentrations in aerosols were determined from the Whatman 41 filters by a microwave digestion scheme with concentrated qd HNO_3 and concentrated HF (*Optima*) described in Morton et al. (2013). Rainwater filtrates, digested seawater particulates, and digested aerosol samples were analyzed by the E2 HR-ICP-MS and Fe concentrations were calculated using matrix-matched external standards calibration. Total aerosol Fe was analyzed on triplicate filters on every other deployment. The precision averaged ± 3.3%. The rain and water column dissolved and particulate Fe measurements were not replicated, but previous work has shown that precision for these methods is typically ± 0.1–0.2 nmol L^{-1}.

Nutrient and organic matter samples were filtered through combusted GF/F filters into 60 mL plastic bottles, which were then frozen. After thawing to room temperature, samples for inorganic nutrients were analyzed on a Seal QuAAtro autoanalyzer. Standard curves with five different concentrations were run daily at the beginning of each run. Fresh standards were made prior to each run by diluting a primary standard with low nutrient surface seawater. MilliQ water was used as a blank, and MilliQ water blanks were run at the beginning and end of each run, as well as after every 8–10 samples to correct for baseline shifts. Method detection limits were 0.02 μmol L^{-1} for NOx and ammonium, and < 0.01 μmol L^{-1} for orthophosphate and silicate. For determination of DOC and TDN concentrations, water samples were analyzed using the High Temperature Catalytic Oxidation method on a Shimadzu TOC-Vs analyzer with nitrogen module. Standard curves were run twice daily using a Deionized water blank and five concentrations of either acid potassium phthalate solution or potassium nitrate for DOC and TDN, respectively. Three to five subsamples were taken from each standard and water sample and injected in sequence. Reagent grade glucosamine was used as a laboratory check standard and inserted throughout each run, as were Certified Reference Material Program (CRMP) deep-water standards of known DOC/TDN concentration. Average daily CRMP DOC and TDN concentrations were 45.2 $\pm$ 7.0 μmol L^{-1} and 31.8 $\pm$ 2.1 μmol L^{-1}, respectively. Dissolved organic nitrogen (DON) was determined by subtracting dissolved inorganic nitrogen (ammonium, NOx) from TDN. For determination of chlorophyll concentrations, a known volume of water sample was gently (≤ 5 mm Hg) filtered through Whatman 25 mm GF/F filters that were then stored frozen until analysis. Chl *a* was extracted from the filters by soaking for 18–24 h in 90% High Performance Liquid Chromatography-grade acetone at −20°C, after which Chl *a* was determined fluorometrically with a Turner Trilogy fluorometer without acidification.

Cell counting

For enumeration of heterotrophic bacteria and picoplankton, 4 mL of sample water was transferred into 5 mL plastic cryovials, 80 μL of 50% glutaraldehyde was added, and vials were stored at −80°C. Samples were thawed at 0°C in the dark and gently filtered through 20 μm Nytex®. Samples for heterotrophic bacteria were stained with SYBR Green I (Marie et al. 1997, 1999). Analysis was done using an Accuri C6 Plus flow cytometer equipped with CSampler Plus. Samples (~ 50 mL) for nanoplankton and microphytoplankton enumeration were preserved with 1 mL formalin and 0.42 mL 2% acid Lugol's. Approximately 25 mL of sample was then settled in Utermohl chambers for at least 25 h. Phytoplankton were enumerated with an inverted microscope at ×200 magnification.

Microbial community analysis

Seawater samples (1 L) were filtered ~ 1 h after collection using Masterflex L/S Precision Modular Drive peristaltic pump (Cole-Parmer, Vernon Hills, IL) with L/S 15 Masterflex tubing through a 5.0 μm Durapore prefilter (EDM Millipore, Darmstadt, Germany) followed by a final filter through a 25 mm 0.22 μm pore-size Durapore membrane to collect the bacterial fraction. Filters were immediately frozen and stored at −80°C until DNA extraction.

Total microbial community DNA was extracted from 0.22 μm filters using a modified version of the EZNA Bacterial DNA kit (Omega Bio-tek, Norcross, GA). Filters were cut into quarters and placed into a single tube for digestion in 20 μL of lysozyme (50 mg mL^{-1}) with 200 μL of 1X TE buffer, and incubated for 30 min with shaking (1000 RPM), at 37°C. After lysozyme treatment, 100 mg sterilized glass beads were added, after which the samples were vortexed at 3000 RPM for 5 min. Two hundred microliters of TL buffer and 40 μL of Proteinase K (20 mg mL^{-1}) were added, and the tubes were incubated at 55°C for 1 h shaking at 600 RPM. Following incubation, samples were processed according to manufacturer's instructions (Manual rev. January 2016), with volumes scaled proportionally as appropriate. Using this method, extraction of blank filters routinely yields DNA concentrations below the detection limit and do not yield detectable amplification of 16S rRNA gene products. Purified DNA was stored at −20°C until Polymerase chain reaction (PCR) amplification and library prep for sequencing.

Library preparation, sequencing, and sequence analysis

The V4 region of the 16S rRNA gene was amplified using a two-step PCR method as described by Tinker and Ottesen (2016). PCR products from all samples were pooled to equimolar concentrations and submitted to the Georgia Genomics Facility for sequencing with custom primers (Caporaso et al. 2012) via manufacturer protocols (Illumina Miseq 250 × 250 base pairs; Illumina, San Diego, CA). Raw sequence data are available from the NCBI Short Read Archive under BioProject PRJNA388812.

Sequence data were processed using the mothur software package (Schloss et al. 2009). The MiSeq standard operating procedure was used with minor modifications: (1) Version 123 of the Silva database (Quast et al. 2013) was used to align the sequences, (2) chimeras were removed using UCHIME (Edgar et al. 2011), (3) the Wang taxonomic classification method was used (Wang et al. 2007), and (4) the sequences were classified using the Green Genes database ver. 13.8 (DeSantis et al. 2006). Because of misassignments in Green Genes, assignment of operational taxonomic units (OTU) to Vibrionales and Alteromonadales was manually verified (Lydon and Lipp 2018). Sequence library sizes and characteristics are presented in Supporting Information - Table S1. Using mothur, sequences were binned into either 97% identity OTUs, which yielded 49,240 total OTUs, or by genus, which yielded 1350 putative genera.

Statistical analyses of microbial community data

DESeq2 (Love et al. 2014) was used to determine significantly changing bacterial taxa from sequence data. To estimate dispersion in gene counts, 16S data from experimental incubation "time zero" samples (collected synoptically with the time series samples but with slightly different handling; see above) were treated as biological replicates of the paired

time series samples, using the "partially replicated experiment" protocol suggested in the DESeq2 documentation. p adjusted values use the Benjamini-Hochberg adjustment.

Nonmetric multidimensional scaling (NMDS) analyses were generated using the vegan package v. 2.4–2 (Oksanen et al. 2007) in R (R Core Team 2016). Vector fitting for environmental data to NMDS and principal components analysis was done using the EnvFit algorithm. p values were based on 10,000 random permutations of sample labels. Spearman's rank correlations were calculated using cor.test in R (Team 2016). Average dust AOT for 24 h (12:00–12:00 h UTC) was correlated against contemporaneously measured subsurface water biological and chemical variables. For analyses between AOT and total and dissolved Fe in collected aerosols, we used the average dust AOT from 18:00 to 18:00 h UTC to align with aerosol collection periods.

24-h incubations of marine surface water for microbial community analysis

In an attempt to determine whether observed changes in microbial community composition were driven by local physicochemical conditions in the water (e.g., dust deposition) or as a consequence of hydrodynamic mixing between water masses carrying different microbial populations, we evaluated changes in microbial community composition over the course of 24 h in experimental incubations of seawater collected on selected days throughout the time series. Water for experimental incubations was collected at the Looe Key Reef site with a peristaltic pump and acid-washed, trace metal free silicone tubing. Tubing inlet was ~ 2 m upcurrent from the boat at ~ 1 m depth. A 200-μm pore-size acid-washed Nitex mesh was placed over the end of the tubing to exclude collection of large debris and *Trichodesmium* clusters. To minimize bottle-to-bottle variability, the water for all experiments was pumped into two acid-washed 50-liter carboys simultaneously. Incubation experiments were started within 3 h of collection.

Incubation experiments were repeated five times on 16, 21, 26, 29, and 31 July 2016 and run in triplicate. After return to shore, 1 L samples were collected from each 50-liter carboy for starting microbial community analyses. For each experiment, seawater was distributed into three different acid-washed 4-liter cubitainers (VWR, Radnor, PA). Samples were incubated using an outdoor, groundwater fed, flow-through incubator with 50% light attenuation. Temperature and light were monitored hourly using HOBO pendant loggers (Onset). After ~ 24 h, samples were dispensed into clean bottles from acid-washed spigots on the cubitainer. One liter from each incubation was used for filtration and microbial community DNA extraction as described above.

Results

Aerosols

During the time series period, both total and dust AOT initially peaked 12–13 July (dust AOT = 0.10), followed by a period of relatively low dust AOT with small peaks noted on 19, 21, and 26 July (Fig. 1). Dust AOT reached a maximum of 0.14 at ~ 00:00 h on 28 July and remained at or above 0.06 through 06 August, the end of the time series (Fig. 1, Supporting Information Table S2). Total aerosol Fe concentrations integrated over each 24-h collection period confirmed some dust influx between 25 and 26 July and higher inputs on 28–29 July, 31 July–01 August, and 03–04 August (Fig. 1). The dust AOT peak on 12–13 July could not be corroborated with aerosol Fe data, as aerosol sample collection did not begin until 15 July. Aerosol Fe concentrations were significantly associated with 24-h averaged total and dust AOT (Spearman's $\rho = 0.73$ and 0.86, respectively, $p < 0.001$ for both). Satellite imagery and wind data were consistent with a Saharan origin for major dust events (Supporting Information Fig. S1). Air mass back trajectory analysis was conducted using the Hysplit model (Stein et al. 2015) and showed trajectories to the east and east-southeast for all aerosol samples (data not shown).

Rainfall events totaling > 10 mm occurred on 20–21, 24–25, 26–29 July, and 02–03 August (Fig. 1). Rainfall-associated dissolved Fe fluxes ranged from 11.6 nmol m^{-2} d^{-1} on 28–29 July to a maximum of 776 nmol m^{-2} d^{-1} on 17–18 July (no measurements of total Fe were conducted). Previous collections of rainwater in the Atlantic Ocean have found that dissolved Fe averages about 8% of total Fe in rainfall samples influenced primarily by Saharan dust input (W. Landing unpubl. data).

Temporal trends in surface water biological and chemical characteristics

Water temperature varied between 29°C and 32°C during the study period (Fig. 1). The warmest temperature (≥ 31°C) was observed from 12 to 14 July, whereas lowest temperatures were observed from 21 to 25 July (Fig. 1), immediately following a period of rain and heavy surf conditions. Salinity was largely stable at 36 ± ~ 0.3 throughout the study period (Fig. 1). DOC concentrations ranging from 89 to 127 μmol L^{-1} were observed between 12 and 14 July (Fig. 1). Concentrations decreased thereafter and remained between 69 and 94 μmol L^{-1} with a spike to 116 μmol L^{-1} on 01 August. DON concentrations peaked on 13 July at 13.2 μmol L^{-1}, then decreased, and remained between 3.6 and 8.9 μmol L^{-1} through the remainder of the study period. Ammonium concentrations ranged from 1.5 to 2.5 μmol L^{-1} with occasional episodic increases, such as on 24 July (4.7 μmol L^{-1}) and 01 August (4.4 μmol L^{-1}). Nitrate concentrations were generally low, with concentrations at or near the detection limit (≤ 0.02 μmol L^{-1}). Noticeable spikes in nitrate concentration occurred 13 July (0.81 μmol L^{-1}), 23–24 July (0.29–0.40 μmol L^{-1}), 29–30 July (0.53–0.75 μmol L^{-1}), and 04 August (0.47 μmol L^{-1}). Orthophosphate concentration was also generally low (< 0.1 μmol L^{-1}) throughout the study period, with exceptions on 16 July (0.2 μmol L^{-1}) and 05 August (0.6 μmol L^{-1}). Silicate concentrations were highly variable during the study, but always < 2.5 μmol L^{-1}.

Total (dissolved and particulate) Fe concentrations in surface waters varied from 5 to 25 nmol L^{-1} early in the study period

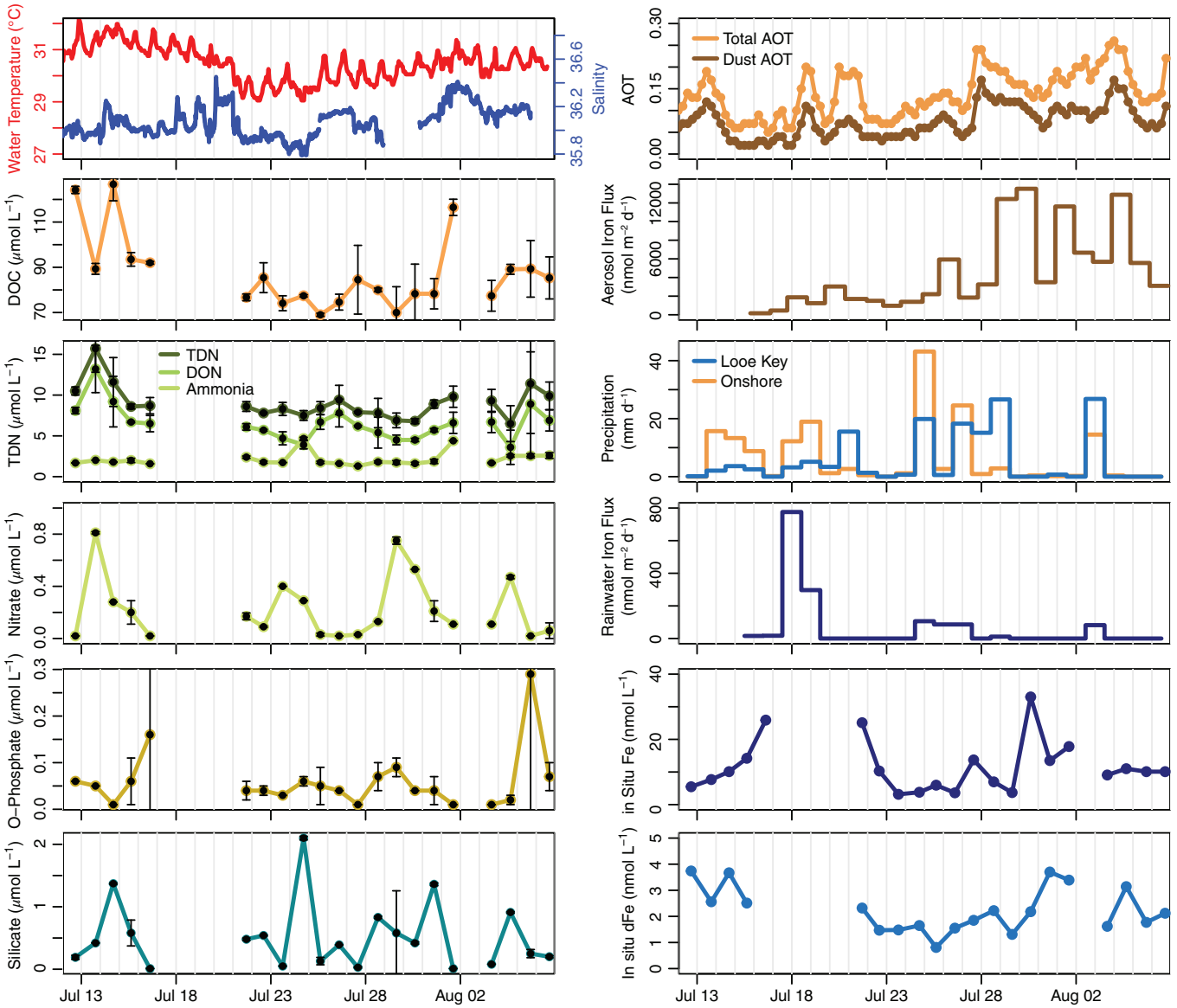

Fig. 1. Measurements of environmental and biological factors during time series. All times are shown in coordinated universal time. Error bars represent the standard deviation of two samples, measurements without error bars were collected in singleton. Total and dust AOT are aerosol optical thickness based on NAAPS model using NASA satellite data. Aerosol iron flux is from 24 h integrated air filter samples using a dry deposition velocity of 1000 m d^{-1}. Precipitation data are based on NAAPS model data for the sample site (blue) and the onshore location (orange) of the rainwater collector used to measure rainwater iron flux in 24 h integrated samples, with the exception of 26–28 July, which was a 48-h integrated sample. Rainwater iron flux is shown as the dissolved iron fraction. In situ Fe represents the sum of dissolved and particulate Fe. In situ dFe represents dissolved Fe (after 0.2 μm filtration).

(12–26 July), including peaks (25 nmol L^{-1}) immediately preceding (16 July) and following (21 July) the sampling gap (Fig. 1). Total Fe concentrations exhibited a small peak on 27 July (13.7 nmol L^{-1}), and a larger peak on 30 July (33 nmol L^{-1}). Dissolved Fe in the water column was relatively high on 12–16 July (2.5–3.4 nmol L^{-1}), then decreased to a local minimum on 25 July (0.8 nmol L^{-1}). This was followed by a peak on 28 July (2.2 nmol L^{-1}), a dip on 29 July (1.3 nmol L^{-1}), and an additional peak 31 July (3.7 nmol L^{-1}).

Across the time series, pFe and dFe in the water column were significantly correlated (Spearman's ρ = 0.46, p = 0.04). Additionally, both measures were significantly associated with aerosol Fe flux (ρ = 0.57, p = 0.04 for pFe and ρ = 0.53 and p = 0.02 for dFe) from the previous day (~ 18 h time lag from endpoint of aerosol sampling) but not the sample contemporaneous with collection. Dissolved (but not particulate) Fe was also significantly associated with aerosol Fe with a 2-d time lag (~ 42 h from endpoint of aerosol sampling; ρ = 0.6, p = 0.02).

Both particulate (ρ = 0.55, p = 0.01) and dissolved (ρ = 0.63, $p < 0.01$) Fe were significantly associated with modeled dust AOT (24-h average) with a 48 h time lag (from endpoint of 24 h window) but not with contemporaneous or 1-d time lagged data.

In situ changes in bacterial and phytoplankton abundance

Relatively high Chl *a* concentrations (≥ 0.5 μg L^{-1}) were observed on 12 and 14–16 July (Fig. 2). Lower Chl *a* concentrations (< 0.3 μg L^{-1}) were observed from 21 to 29 July. Chl *a* increased sharply from 31 July to 01 August, reaching 1.5 μg L^{-1} (Fig. 2). Chl *a* decreased after 01 August and was < 0.4 μg L^{-1} for the rest of the study period.

At the beginning of the study, photosynthetic picoeukaryote and picocyanobacteria abundances were nearly equivalent (~ 4×10^4 cells mL^{-1}). Abundances of both increased beginning 13–14 July, reaching 5.4–5.6 $\times 10^4$ cells mL^{-1} (Fig. 2). Thereafter, picocyanobacteria abundance continued to increase sharply and peaked on 16 July at 7.8×10^4 cells mL^{-1}, while picoeukaryote abundance decreased to 1.9×10^4 cells mL^{-1} on 16 July (Fig. 2). Both picoeukaryote and picocyanobacteria abundances were much lower on the next sampling date, 21 July, but increased later in the time series. Picoeukaryote abundances reached 1.1×10^5 cells mL^{-1} on 29 July. Picocyanobacteria abundances remained relatively low until 30 July, after which they increased to a maximum abundance of 5.9×10^4 cells mL^{-1} on 04 August. A relatively high abundance of the diatom *Chaetoceros* was observed on 12 July at 157 cells mL^{-1} (Fig. 2). Late in the monitoring period, a rapid increase in *Chaetoceros* abundance occurred, reaching 430 cells mL^{-1} on 01 August (Fig. 2).

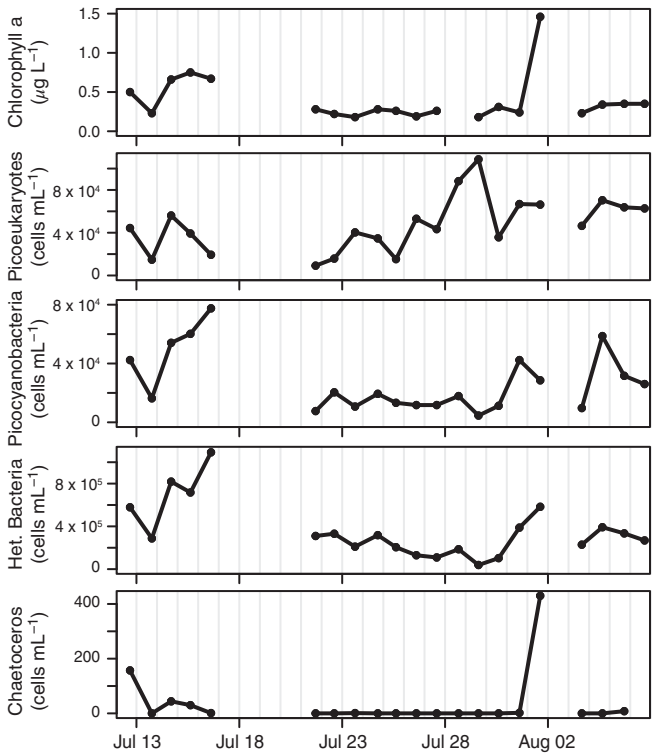

Fig. 2. Time series of Chl *a* and abundances of picoeukaryotic phytoplankton, picocyanobacteria, heterotrophic bacteria, and *Chaetoceros* sp.

The concentration of heterotrophic bacteria largely tracked that of picocyanobacteria (Fig. 2). Across the time series, these groups were strongly associated (Spearman's $\rho = 0.85$, $p < 0.001$). Total heterotrophic bacteria abundance was 5.8×10^5 cells mL^{-1} on 12 July, decreased to 2.9×10^5 cells mL^{-1} on 13 July, and then increased to a peak of 1.1×10^6 cells mL^{-1} on 16 July. When sampling resumed on 21 July, heterotrophic bacterial abundances had fallen substantially, and continued to decline until reaching a minimum of 3.9×10^4 cells mL^{-1} on 29 July. Thereafter, they increased in abundance with a peak at 5.8×10^5 cells mL^{-1} on 01 August.

We observed positive relationships between picoeukaryote abundances and salinity, aerosol total Fe, and total and dust AOT (Table 1). Picocyanobacteria and heterotrophic bacteria abundances were positively associated with DOC, Chl *a*, water column dFe, and water temperature. Finally, significant positive associations were identified between concentrations of *Chaetoceros* and DOC, water temperature, Chl *a*, water column dFe, and TDN.

Bacterial community composition and temporal dynamics

Bacterial community composition analysis revealed a temporally dynamic community (Fig. 3). NMDS ordination analyses show that community composition clustered by time of collection, with the first five samples (12–16 July) clustering together, followed by a second cluster representing samples collected from 21 to 24 July (after the 4-d sampling gap). Starting on 25 July, strong shifts in overall community composition were observed, with all samples collected in the later sampling period clustering in the upper portion of the ordination plot. Ordinations showed strong relationships ($p < 0.01$) between community composition and dust AOT, water column dFe, water temperature, and DOC.

Figure 4 shows dynamics in the relative abundance of genera representing > 5% of the community, while Fig. 5 shows temporal dynamics in selected genera. During the initial 5 d of sampling (12–16 July), *Synechococcus* was the most abundant cyanobacterium, while the most abundant heterotrophic taxa were unclassified *Flavobacteriaceae*, *Halomonadaceae*, and *Acidimicrobiales*. Following the 16–21 July sampling gap, the microbial community was found to have shifted substantially. Samples collected 21–24 July, which cluster tightly in ordination analyses (Fig. 3), showed decreased relative abundances of *Synechococcus* and *Flavobacteriaceae*, and a substantial increase in the relative abundance of unclassified *Pelagibacteraceae* and *Prochlorococcus*.

The remainder of the time series showed a series of progressive shifts in bacterial community composition. The relative abundance of *Pelagibacteraceae* began declining on the 25 July, and between 24 July and 01 August saw a 24-fold decrease (p adjusted ≤ 0.001) in relative abundance. Generally, the dominant cyanobacterial groups (*Prochlorococcus* and *Synechococcus*) showed inverse relationships. The relative abundance of *Prochlorococcus* increased slightly from 24 to 26 July and peaked at 11%

Table 1. Relationships between physical, chemical, and biological variables. Spearman rank correlations between environmental and biological variables.

	Chl *a*	Picoeukaryotes	Picocyanobacteria	Heterotrophic bacteria	*Chaetoceros*
Total AOT	−0.11	0.51*	−0.31	−0.28	−0.30
Dust AOT	−0.09	0.58*	−0.22	−0.29	−0.21
Aerosol total Fe	0.07	0.63*	−0.08	−0.23	−0.08
Rainwater dFe	−0.31	−0.18	−0.28	−0.39	−0.28
Water total Fe	0.57*	−0.17	0.33	0.38	0.17
Water dFe	0.66*	0.20	0.63*	0.66*	0.56*
Temperature	0.64*	0.18	0.60*	0.61*	0.61*
Salinity	0.32	0.65*	0.07	0.12	0.25
DOC	0.77*	0.09	0.78*	0.77*	0.65*
TDN	0.30	−0.02	0.28	0.41	0.52*
DON	0.27	−0.14	0.23	0.28	0.37
Ammonia	0.31	0.16	0.28	0.36	0.11
Nitrate	−0.27	0.05	−0.24	−0.16	−0.21
Nitrite	−0.27	−0.29	−0.26	−0.22	−0.02
O-Phosphate	0.13	0.02	0.19	0.01	−0.02
Silicate	−0.09	0.21	0.16	0.09	−0.15
Chl *a*	1.00	0.09	0.72*	0.73*	0.61*

*Correlations with p value < 0.05.

of recovered reads; it then decreased rapidly, experiencing a 23-fold decrease between 28 July and 01 August ($p < 0.001$). Conversely, *Synechococcus* increased in relative abundance from 4.3% on 28 July to a peak of 21.2% on 31 July and remained at 15–25% of sequences for the remainder of the time series, with the exception of a local minimum at 7.8% on 03 August.

The decrease in overall bacterial abundance observed on 29 July was accompanied by a large increase in bacterial diversity (Fig. 5). On this date, OTU richness peaked at 7657 from a previous average of 1870 (12–28 July). Similarly, the proportion of rare taxa (taxa observed at a relative abundance of < 5% in all samples) averaged 27% of the total bacterial community from 12 to 28 July, but peaked at 44% of the community on 29 July, then decreased again to an average of 24% from 30 July to 06 August. The increase in relative abundance of rare taxa translated to an increase in Shannon diversity from an average of 4.07–5.39 on 29 July before declining to 3.91. As an example, a single rare OTU, identified as an unclassified member of the *Vibrionales* order, increased significantly from 28 to 29 July, as well as from 12 to 13 July (Fig. 5, Supporting Information Table S3).

The period following the most intense dust event observed, 28–29 July, was marked by a series of progressive blooms in heterotrophic bacterial taxa (Figs. 4,5). Following the early increase in typically rare taxa like Vibrionales (29 July), the next group to peak was an unclassified member of the *Cryomorphaceae* family, which increased from a low of 0.5% on July 24 to a peak of 6.8% on 30 July. Subsequently, between 30 and 31 July, an unclassified OTU belonging to the *Rhodobacteraceae* showed a sharp increase (3.72-fold, p adjusted ≤ 0.001). Finally, an unclassified member of the *Flavobacteriaceae* family increased 2.63-fold (p adjusted = 0.0018) on 01 August, whereon it became the single most abundant bacterial taxon identified, at 24% of the community.

Incubation experiments

A key difficulty in analysis of field-collected microbial community composition data is distinguishing microbial community responses to environmental variables (e.g., dust, nutrients, etc.) from microbial community shifts resulting from hydrodynamic mixing between water masses carrying different microbial populations. In order to separate these factors, we evaluated changes in microbial community composition over the course of 24 h in experimental incubations of seawater collected on selected days throughout the time series. As these experimental microcosms were closed and thus isolated from further microbial inputs, any shifts in microbial community composition were assumed to be the result of microbial growth responses to local physicochemical conditions captured at time of collection (e.g., dust inputs), particularly when similar responses were observed both in situ and in our incubations. Water collected on 16, 26, and 31 July showed very few changes in microbial community composition following incubation under ambient conditions, with only 1, 2, and 4 - microbial taxa, respectively, exhibiting statistically significant changes in abundance over the 24-h period (Fig. 6, Supporting Information Table S4).

Conversely, incubation experiments initiated on 21 and 29 July saw much larger changes in the microbial community. Twenty-nine genera exhibited significant changes in abundance during incubation of the water collected on 21 July, with 17 of

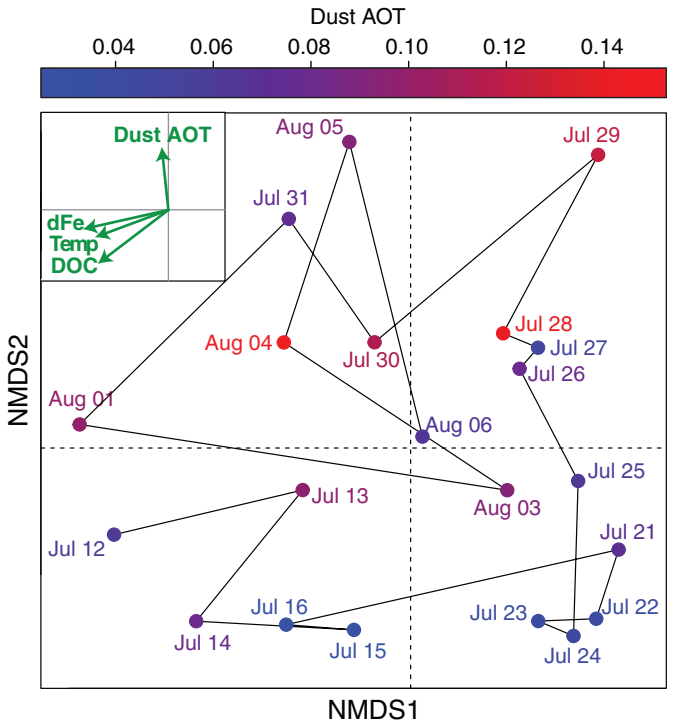

Fig. 3. NMDS plot of bacterial community similarity (based on genus-level phylotype abundance) with correlated environmental measurements. NMDS analysis used Bray-Curtis dissimilarity without auto transformation. Black lines connect samples collected on consecutive days (to show the temporal progression of the community). Color of points/dates indicates dust AOT. Inset shows environmental factors that are strongly correlated with community shifts ($p < 0.01$), dFe: water column dissolved iron. Total AOT, aerosol iron content, and salinity were also found to be correlated with $p < 0.05$. Rainwater iron flux, water column total iron, TDN, DON, ammonia, nitrate, nitrite, orthophosphate, and silicate did not show a significant relationship. All libraries were resampled to a constant depth of 33,086 sequences.

the 29 genera that changed belonging to the *Proteobacteria* (Supporting Information Table S4). Incubations of water collected on 29 July, following substantial dust deposition, exhibited 51 genera with significantly changing relative abundances. Six of the eight genera that significantly changed in the in situ time series from 29 to 30 July also changed in the incubations (Supporting Information Table S3). Genera highlighted in Fig. 5 that were identified as showing significant changes in the 29 July incubation and that exhibited similar dynamics 29 July–01 August in situ included *Synechococcus*, *Prochlorococcus*, a *Cryomorphaceae* bacterium, and a *Rhodobacteraceae* bacterium (Supporting Information Tables S3, S4).

Discussion

Prevailing easterly winds bring air masses across the Atlantic from western Africa in the summer that contribute large amounts of dust in pulses lasting 3–5 d (Prospero 2007). In the summer, these aerosols are transported to the Caribbean and tropical/subtropical western Atlantic. Although the frequency at which dust events reach the southeastern U.S. (e.g., Florida Keys) may vary, typically multiple dust events can be expected between July and August (Perry et al. 1997). In this work, we present a time series documenting atmospheric dust content and aerosol iron concentrations, water column nutrient, carbon, and iron concentrations, phytoplankton and bacterioplankton abundances, and bacterial community composition in surface waters at Looe Key Reef (Florida, U.S.A.), following trans-Atlantic transport. Modeled AOT and measured aerosol concentration of Fe (Fig. 1) indicate that our study included at least three dust events. AOT estimates suggest that we captured a dust event at the initiation of our time series (12 July), although aerosol data were not available until 15 July. Both AOT and aerosol measurements suggest that we captured a small dust event on 25–26 July 2016 that was accompanied by rainfall-associated "wet" deposition of Fe (and dust) and a strong event on 28–29 July, followed by generally elevated dust levels for the remainder of the time series. Dust flux calculations are consistent with additional significant dust inputs 31 July–01 August and 03–04 August, although generally elevated dust levels during this time may have altered microbial community responses to these dust influxes. Each dust event was associated with distinct microbial community dynamics that nonetheless showed some marked similarity.

One of the more notable relationships throughout the time series was a consistent pattern in which dust deposition was accompanied by a bloom in picoeukaryote cellular abundance followed by a later peak in heterotrophic bacteria and picocyanobacteria abundances. In a mesocosm study using waters from a transect of the central North Atlantic, Marañén et al. (2010) also reported picoeukaryote abundance typically increased within 48 h of dust addition to surface water, while cyanobacteria and heterotrophic bacteria typically decreased or remained constant. In contrast, studies using Mediterranean seawater have reported either concurrent growth of picoeukaryotes and cyanobacteria (Lagaria et al. 2017), or no change in picoeukaryote abundance and delayed growth of cyanobacteria (Giovagnetti et al. 2013).

These shifts in cellular abundance were accompanied by changes in bacterial community composition. *Pelagibacteraceae* and *Prochlorococcus* relative abundance typically decreased coincident with dust deposition, while successive growth of *Vibrionales*, *Cryomorphaceae*, *Rhodobacteraceae*, and *Synechococcus* were often observed after deposition. Decreases in abundance and metabolic responses in *Pelagibacter* and *Prochlorococcus* after particulate dust addition both in situ after 90 h (Herut et al. 2005), and in experimental microcosm incubations after 2 d incubations (Hill et al. 2010; Marín et al. 2017) have been previously reported in other systems. The relative abundance of *Vibrionales* increased within 1 d of dust deposition, consistent with earlier findings in this system (Westrich et al. 2016, 2018). These early responders are typically found in low abundance in marine systems, but are known to opportunistically respond to newly available nutrients and substrate (Takemura et al. 2014). As the blooms in *Vibrionales* declined, *Cryomorphaceae* relative abundances increased. To our knowledge, this is the first report

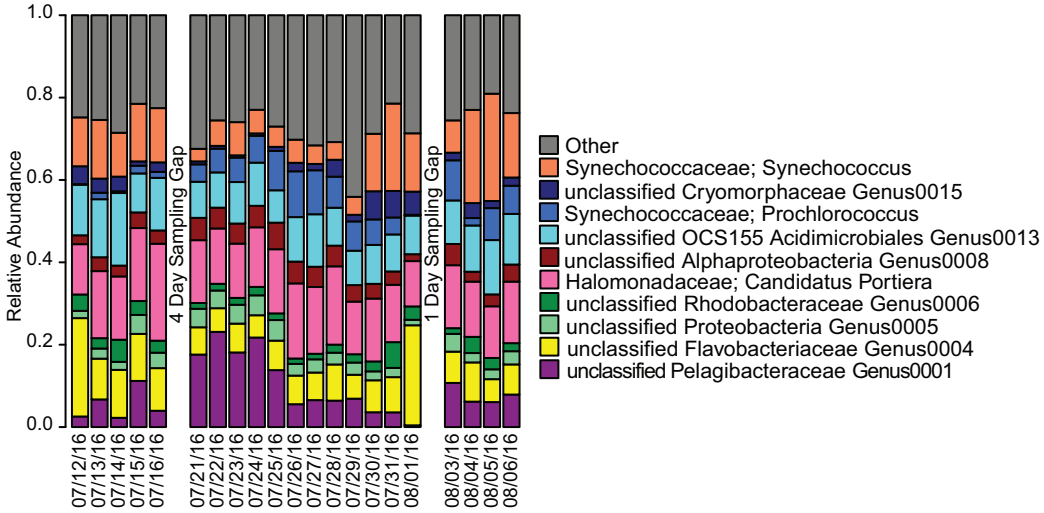

Fig. 4. Bacterial community composition throughout the time series. Colored bars show the relative abundance of any bacterial genus that is > 5% of any one sample, with taxa < 5% of samples combined into gray portion. Sequences not classified at the genus level are labeled with OTU numbers to allow cross-referencing of taxa across figures and tables.

of *Cryomorphaceae* growth following atmospheric dust deposition. *Cryomorphaceae*, which were first observed as uncultured bacteria associated with marine aggregates (Delong et al. 1993; Bowman 2014), have been implicated as secondary degraders of organic carbon (Bowman 2014) and may have taken advantage of decline in preceding blooms of picoeukaryotes or *Vibrionales*. Following (31 July) or synchronously (14 July, 04 August) with the *Cryomorphaceae*, *Rhodobacteriaceae* also increased. Members of the *Rhodobacteraceae* were previously shown to increase in microcosm experiments conducted in the Mediterranean after atmospheric dust input (Guo et al. 2016), although the response reported in that study was immediate (within 3 h). *Rhodobacteraceae* are known to acquire and use a wide variety of substrates for growth (Moran et al. 2007), including bacterial and phytoplankton lysates, whose availability following dust deposition is likely to vary with differential community responses.

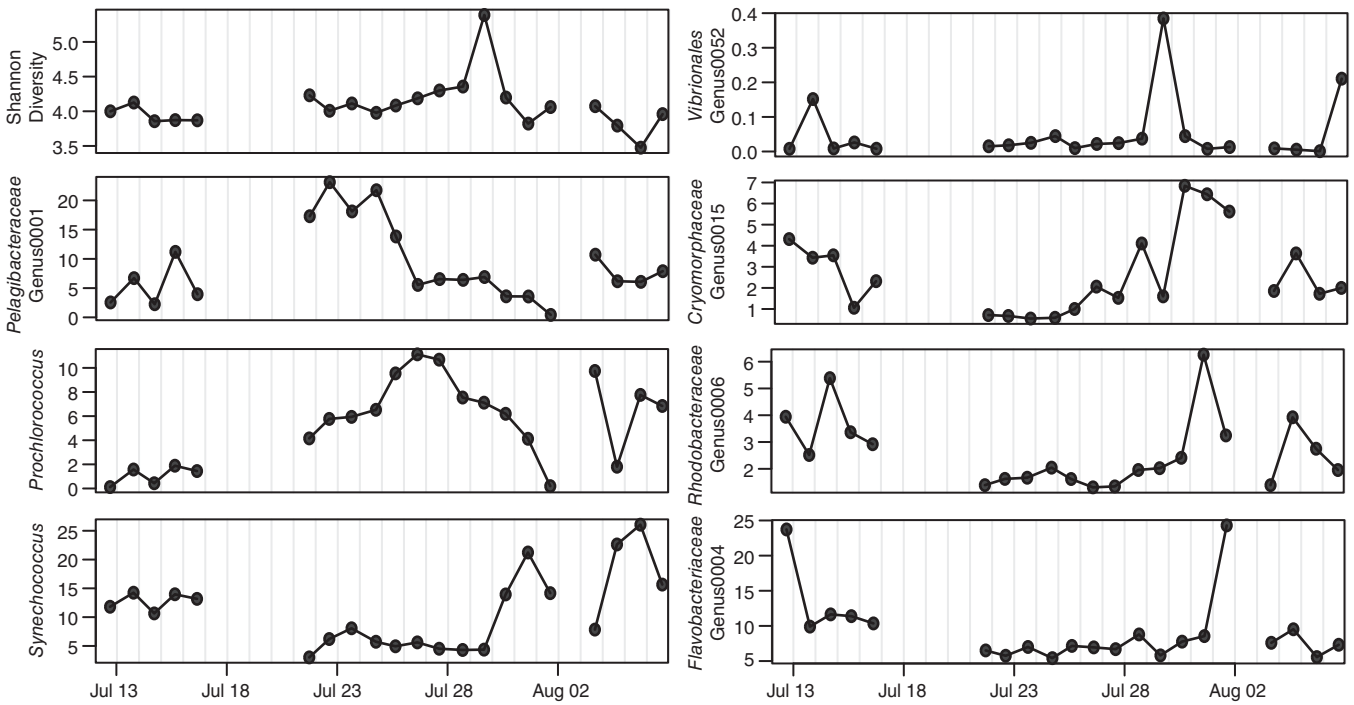

Fig. 5. Time series showing temporal dynamics in the Shannon diversity index and the relative abundances of selected genus-level groups. Shannon diversity index calculated at the 97% OTU level. All other graphs show relative abundances of genus-level taxa as percent of sequence reads.

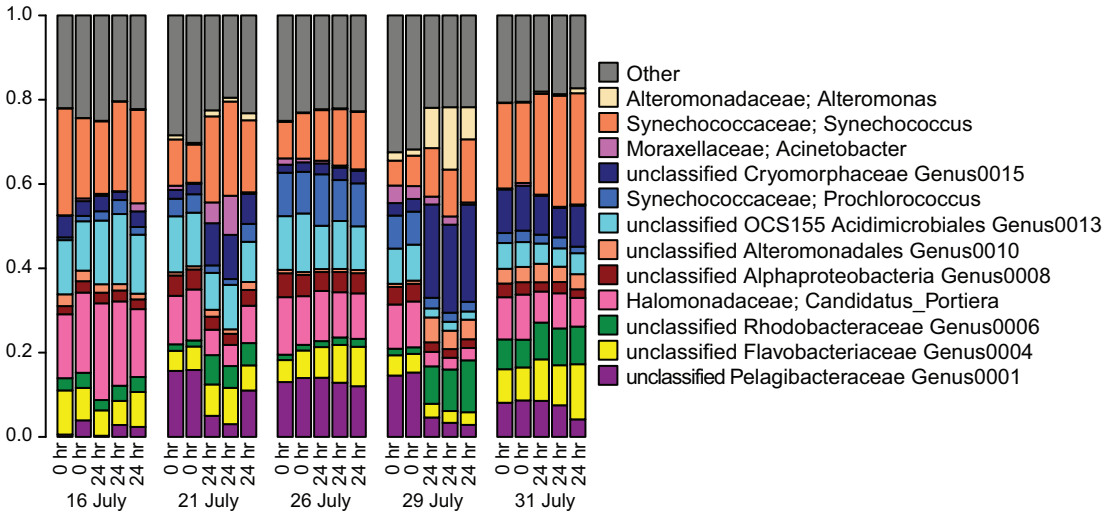

Fig. 6. Relative abundance of bacterial genera in surface-water incubation experiments. Genera representing > 5% of sequences in any one sample are shown. Incubations used water collected on 16, 21, 26, 29, and 31 July. On each date, two replicate samples were collected preincubation, and three replicate incubations were held for 24 h to observe changes in community composition over time.

Finally, 3–4 d after dust input, *Synechococcus* bloomed. *Synechococcus* growth following dust addition has been previously reported (Herut et al. 2005; Ridame et al. 2014; Lagaria et al. 2017; Marín et al. 2017), although others have reported decreases (Paytan et al. 2009; Marañén et al. 2010), potentially due to copper toxicity (Paytan et al. 2009).

Similar changes in microbial community composition to those observed in situ were documented in incubated seawater that was collected on 29 July (immediately following peak dust deposition). These responses are unlikely to be a result of our incubation conditions, as seawater collected at other points within the time series did not exhibit similar alterations in community composition after incubation. While this does not represent an explicit causal link between dust deposition and observed community responses, it strongly suggests that the microbial community changes observed 29–30 July were a response to physicochemical conditions already present in the water on 29 July, rather than the result of hydrodynamic mixing between water masses carrying different microbial communities.

Across the time series, water column dissolved and total iron exhibited a 24–48 h time-delayed relationship with atmospheric dust and aerosol iron concentrations that is suggestive of bioprocessing. We note that, within our time series, picoeukaryote abundance was associated with atmospheric dust content (dust AOT and aerosol total Fe), suggesting a rapid response to the deposition event. Over a similar timescale, the bacterial community composition began to shift with an increase in the relative abundance of *Vibrionales*. However, the total concentrations of both cyanobacteria and heterotrophic bacteria lagged the deposition period and were instead associated with dissolved iron in seawater rather than aerosols. The interactions between picoeukaryotes and cyanobacterial and heterotrophic bacterial concentrations as well as the consistent successional response to dust could be based on biological processing of iron or other nutrients in atmospherically transported dust. At least some groups of photosynthetic picoeukaryotes are capable of phagocytosis of small particles (McKie-Krisberg and Sanders 2014). It seems plausible that phagocytosis of dust particulates could increase the retention time of dust particles at the sea surface. Lysis or incomplete predation of these phytoplankton, as well as excretion of partially digested particles and/or production of organically bound Fe (ligands), could explain the time-delayed increases in seawater particulate and dissolved iron, which in turn could then have fueled the growth of picocyanobacteria and heterotrophic bacterial groups. Alternatively, in both bloom periods, cyanobacteria growth corresponded with warmer water temperatures. Picocyanobacterial abundance was correlated with temperature across the time series (Table 1), and picocyanobacteria have previously been shown to be particularly sensitive to water temperature, whereas picoeukaryote growth is less so (Kuosa 1991; Agawin et al. 1998). However, these temperature relationships do not explain the temporal delay between atmospheric dust inputs and increases in particulate and dissolved iron concentrations, which are suggestive of bioaccumulation and bioprocessing.

Ecological implications

Findings from this study highlight the many impacts that deposition of Saharan dust has on the nearshore microbial community in this subtropical ecosystem, following trans-Atlantic transport and processing of dust aerosols. Because atmospheric processing appears to increase the solubility of aerosol Fe, the quality and quantity of dust aerosols researching these surface communities are likely to be distinct from those of the Mediterranean or the tropical Atlantic closer to the Saharan dust source (Mahowald et al. 2005; Baker and Croot 2010; Longo et al. 2016; Mahowald et al. 2018). Dust deposition events

were followed by strong changes in phytoplankton abundance and bacterial community composition. Our observations are consistent with earlier work that suggested *Vibrio*, likely enhanced by a large repertoire of Fe acquisition mechanisms, are early heterotrophic responders to dust (e.g., Westrich et al. 2016), but expands this finding to reveal both repeatable successional changes in the community over time and the novel early response of picoeukaryotes to dust. Our observations suggest that picoeukaryotes play a key role in the initial processing of dust but are lost over time, and that this tradeoff in dominant phytoplankton is accompanied by progressive changes in the heterotrophic bacterial community. Furthermore, the presence of a temporal delay between increases in aerosol iron concentrations and increases in seawater dissolved and particulate iron suggests that biological accumulation and/or transformation of iron may play an important role in shaping marine responses to atmospheric dust inputs. These relationships may be critical to understand the impacts of dust deposition on marine microbial community structure and function. As an example, while *Vibrio* growth following dust deposition has been observed in situ (Westrich et al. 2016, 2018), incubation experiments suggest that high concentrations of dust leachate must be added to seawater to stimulate this growth (Zhang et al. 2019), suggesting that dust events large enough to stimulate substantial *Vibrio* blooms are likely to be rare. However, if picoeukaryotes and/or other members of the marine microbial community are able to process particulate iron into a more bioavailable form, then model predictions based on growth responses to dust leachate/soluble Fe could substantially underestimate bloom frequency. These intriguing findings, along with recent work suggesting alteration of dust transport magnitude due to climate change (Evan et al. 2016), provide impetus for additional studies to elucidate the role of dust-borne nutrients and water temperature in regulating phytoplankton and bacterioplankton growth and microbial community composition in subtropical ecosystems such as this region of the Florida Keys.

References

Agawin, N. S. R., C. M. Duarte, and S. Agust. 1998. Growth and abundance of *Synechococcus* sp. in a Mediterranean Bay: Seasonality and relationship with temperature. Mar. Ecol. Prog. Ser. **170**: 45–53. doi:10.3354/meps170045

Astrahan, P., B. Herut, A. Paytan, and E. Rahav. 2016. The impact of dry atmospheric deposition on the sea-surface microlayer in the SE Mediterranean Sea: An experimental approach. Front. Mar. Sci. **3**: 222. doi:10.3389/fmars.2016.00222

Baker, A. R., and P. L. Croot. 2010. Atmospheric and marine controls on aerosol iron solubility in seawater. Mar. Chem. **120**: 4–13. doi:10.1016/j.marchem.2008.09.003

Bowman, J. P. 2014, p. 539–550. *In* E. Rosenberg, E. F. DeLong, S. Lory, E. Stackebrandt, and F. Thompson [eds.], The family Cryomorphaceae. Springer: The prokaryotes.

Bruland, K. W., R. P. Franks, G. A. Knauer, and J. H. Martin. 1979. Sampling and analytical methods for the determination of copper, cadmium, zinc, and nickel at the nanogram per liter level in sea-water. Anal. Chim. Acta **105**: 233–245. doi:10.1016/S0003-2670(01)83754-5

Caporaso, J. G., and others. 2012. Ultra-high-throughput microbial community analysis on the Illumina HiSeq and MiSeq platforms. ISME J. **6**: 1621–1624. doi:10.1038/ismej.2012.8

Davey, M., G. A. Tarran, M. M. Mills, C. Ridame, R. J. Geider, and J. LaRoche. 2008. Nutrient limitation of picophytoplankton photosynthesis and growth in the tropical North Atlantic. Limnol. Oceanogr. **53**: 1722–1733. doi:10.4319/lo.2008.53.5.1722

DeLong, E. F., D. G. Franks, and A. L. Alldredge. 1993. Phylogenetic diversity of aggregate-attached vs. free-living marine bacterial assemblages. Limnol. Oceanogr. **38**: 924–934. doi:10.4319/lo.1993.38.5.0924

DeSantis, T. Z., and others. 2006. Greengenes, a chimera-checked 16S rRNA gene database and workbench compatible with ARB. Appl. Environ. Microbiol. **72**: 5069–5072. doi:10.1128/AEM.03006-05

Duarte, C. M., and others. 2006. Aerosol inputs enhance new production in the subtropical northeast Atlantic. J. Geophys. Res. Biogeosci. **111**:G04006. doi:10.1029/2005JG000140

Ebling, A. M., and W. M. Landing. 2015. Sampling and analysis of the sea surface microlayer for dissolved and particulate trace elements. Mar. Chem. **177**: 134–142. doi:10.1016/j.marchem.2015.03.012

Edgar, R. C., B. J. Haas, J. C. Clemente, C. Quince, and R. Knight. 2011. UCHIME improves sensitivity and speed of chimera detection. Bioinformatics **27**: 2194–2200. doi:10.1093/bioinformatics/btr381

Evan, A. T., C. Flamant, M. Gaetani, and F. Guichard. 2016. The past, present and future of African dust. Nature **531**: 493–495. doi:10.1038/nature17149

Giovagnetti, V., and others. 2013. Assessing the role of dust deposition on phytoplankton ecophysiology and succession in a low-nutrient low-chlorophyll ecosystem: A mesocosm experiment in the Mediterranean Sea. Biogeosciences **10**: 2973–2991. doi:10.5194/bg-10-2973-2013

Guieu, C., and others. 2010. Large clean mesocosms and simulated dust deposition: A new methodology to investigate responses of marine oligotrophic ecosystems to atmospheric inputs. Biogeosciences **7**: 2765–2784. doi:10.5194/bg-7-2765-2010

Guieu, C., C. Ridame, E. Pulido-Villena, M. Bressac, K. Desboeufs, and F. Dulac. 2014. Dust deposition in an oligotrophic marine environment: Impact on the carbon budget. Biogeosci. Discuss. **11**: 1707–1738. doi:10.5194/bgd-11-1707-2014

Guo, C., and others. 2016. Shifts in microbial community structure and activity in the ultra-oligotrophic Eastern Mediterranean Sea driven by the deposition of Saharan dust and European aerosols. Front. Mar. Sci. **3**: 1–13. doi:10.3389/fmars.2016.00170

Herut, B., and others. 2005. Response of East Mediterranean surface water to Saharan dust: On-board microcosm experiment and field observations. Deep-Sea Res. Part II Top. Stud. Oceanogr. **52**: 3024–3040. doi:10.1016/j.dsr2.2005.09.003

Hill, P. G., M. V. Zubkov, and D. A. Purdie. 2010. Differential responses of Prochlorococcus and SAR11-dominated bacterioplankton groups to atmospheric dust inputs in the tropical Northeast Atlantic Ocean. FEMS Microbiol. Lett. **306**: 82–89. doi:10.1111/j.1574-6968.2010.01940.x

Kuosa, H. 1991. Picoplanktonic algae in the northern Baltic Sea: Seasonal dynamics and flagellate grazing. Marine Ecology Progress Series **73**: 269–276. doi:10.3354/meps073269

Lagaria, A., and others. 2017. Phytoplankton response to Saharan dust depositions in the Eastern Mediterranean Sea: A mesocosm study. Front. Mar. Sci. **3**: 1–16. doi:10.3389/fmars.2016.00287

Laghdass, M., S. Blain, M. Besseling, P. Catala, C. Guieu, and I. Obernosterer. 2011. Effects of Saharan dust on the microbial community during a large in situ mesocosm experiment in the NW Mediterranean Sea. Aquat. Microb. Ecol. **62**: 201–213. doi:10.3354/ame01466

Langlois, R. J., M. M. Mills, C. Ridame, P. Croot, and J. LaRoche. 2012. Diazotrophic bacteria respond to Saharan dust additions. Mar. Ecol. Prog. Ser. **470**: 1–14. doi:10.3354/meps10109

Lee, S., and J. A. Fuhrman. 1991. Species composition shift of confined bacterioplankton studied at the level of community DNA. Mar. Ecol. Prog. Ser. **79**: 195–201. doi:10.3354/meps079195

Lekunberri, I., and others. 2010. Effects of a dust deposition event on coastal marine microbial abundance and activity, bacterial community structure and ecosystem function. J. Plankton Res. **32**: 381–396. doi:10.1093/plankt/fbp137

Lenes, J. M., and others. 2001. Iron fertilization and the *Trichodesmium* response on the West Florida shelf. Limnol. Oceanogr. **46**: 1261–1277. doi:10.4319/lo.2001.46.6.1261

Lin, Y. 2011. GCIP/EOP surface: Precipitation NCEP/EMC 4KM gridded data (GRIB) stage IV data. UCAR/NCAR – Earth Observing Laboratory. doi:10.5065/D69Z93M3

Longo, A. F., and others. 2016. Influence of atmospheric processes on the solubility and composition of iron in Saharan dust. Environ. Sci. Technol. **50**: 6912–6920. doi:10.1021/acs.est.6b02605

Love, M. I., W. Huber, and S. Anders. 2014. Moderated estimation of fold change and dispersion for RNA-seq data with DESeq2. Genome Biol. **15**: 550–550. doi:10.1186/s13059-014-0550-8

Lydon, K. A., and E. K. Lipp. 2018. Taxonomic annotation errors incorrectly assign the family Pseudoalteromonadaceae to the order Vibrionales in greengenes: Implications for microbial community assessments. PeerJ **6**: e5248. doi:10.7717/peerj.5248

Lynch, P., and others. 2016. An 11-year global gridded aerosol optical thickness reanalysis (v1.0) for atmospheric and climate sciences. Geosci. Model Dev. **9**: 1489–1522. doi:10.5194/gmd-9-1489-2016

Mahowald, N. M., and others. 2005. Atmospheric global dust cycle and iron inputs to the ocean. Global Biogeochem. Cycles **19**: 1–15. doi:10.1029/2004GB002402

Mahowald, N. M., and others. 2018. Aerosol trace metal leaching and impacts on marine microorganisms. Nat. Commun. **9**: 2614. doi:10.1038/s41467-018-04970-7

Marañén, E., and others. 2010. Degree of oligotrophy controls the response of microbial plankton to Saharan dust. Limnol. Oceanogr. **55**: 2339–2352. doi:10.4319/lo.2010.55.6.2339

Marie, D., F. Partensky, S. Jacquet, and D. Vaulot. 1997. Enumeration and cell cycle analysis of natural populations of marine picoplankton by flow cytometry using nucleic acid stain SYBR Green I. Appl. Environ. Microbiol. **63**: 186–193.

Marie, D., F. Partensky, D. Vaulot, and C. Brussaard. 1999. Enumeration of phytoplankton, bacteria, and viruses in marine samples. Curr. Protoc. Cytom. **10**: 11.11.1–11.11.15. doi:10.1002/0471142956.cy1111s10

Marín, I., and others. 2017. Anthropogenic versus mineral aerosols in the stimulation of microbial planktonic communities in coastal waters of the northwestern Mediterranean Sea. Sci. Total Environ. **574**: 553–568. doi:10.1016/j.scitotenv.2016.09.005

Massana, R., C. Pedrós-Alió, E. O. Casamayor, and J. M. Gasol. 2001. Changes in marine bacterioplankton phylogenetic composition during incubations designed to measure biogeochemically significant parameters. Limnol. Oceanogr. **46**: 1181–1188. doi:10.4319/lo.2001.46.5.1181

McKie-Krisberg, Z. M., and R. W. Sanders. 2014. Phagotrophy by the picoeukaryotic green alga micromonas: Implications for Arctic Oceans. ISME J. **8**: 1953–1961. doi:10.1038/ismej.2014.16

Mills, M. M., C. Ridame, M. Davey, J. La Roche, and R. J. Geider. 2004. Iron and phosphorus co-limit nitrogen fixation in the eastern tropical North Atlantic. Nature **429**: 292–294. doi:10.1038/nature02550

Moran, M. A., and others. 2007. Ecological genomics of marine roseobacters. Appl. Environ. Microbiol. **73**: 4559–4569. doi:10.1128/AEM.02580-06

Morton, P. L., and others. 2013. Methods for the sampling and analysis of marine aerosols: Results from the 2008 GEOTRACES aerosol intercalibration experiment. Limnol. Oceanogr. **11**: 62–78. doi:10.4319/lom.2013.11.62

Moxim, W. J., S. M. Fan, and H. Levy. 2011. The meteorological nature of variable soluble iron transport and deposition within the North Atlantic Ocean basin. J. Geophys. Res. Atmos. **116**: 1–26. doi:10.1029/2010JD014709

Oksanen, J., R. Kindt, P. Legendre, B. O'Hara, and M. H. Stevens. 2007. 'vegan' community ecology package for R. Package version 2.4-4.

Paytan, A., and others. 2009. Toxicity of atmospheric aerosols on marine phytoplankton. Proc. Natl. Acad. Sci. USA **106**: 4601–4605. doi:10.1073/pnas.0811486106

Perry, K. D., T. A. Cahill, R. A. Eldred, D. D. Dutcher, and T. E. Gill. 1997. Long-range transport of North African dust to the eastern United States. J. Geophys. Res. Atmos. **102**: 11225–11238. doi:10.1029/97JD00260

Pitta, P., B. Herut, and T. M. Tsagaraki. 2017*a*. Editorial: Impact of aerosols (Saharan dust and mixed) on the East Mediterranean oligotrophic ecosystem, results from experimental studies. Front. Mar. Sci. **4**: 264. doi:10.3389/fmars.2017.00210

Pitta, P., and others. 2017*b*. Saharan dust deposition effects on the microbial food web in the Eastern Mediterranean: A study based on a mesocosm experiment. Front. Mar. Sci. **4**: 117. doi:10.3389/fmars.2017.00117

Prospero, J. M. 2007. African dust: Its large-scale transport over the Atlantic Ocean and its impact on the Mediterranean region, p, p. 15–38. *In* A. Mellouki and A. R. Ravishankara [eds.], Regional climate variability and its impacts in the Mediterranean area. Springer. doi:10.1007/978-1-4020-6429-6_2

Pulido-Villena, E., T. Wagener, and C. Guieu. 2008. Bacterial response to dust pulses in the western Mediterranean: Implications for carbon cycling in the oligotropic ocean. Global Biogeochem. Cycles **22**: 1–12. doi:10.1029/2007GB003091

Pulido-Villena, E., and others. 2014. Microbial food web dynamics in response to a Saharan dust event: Results from a mesocosm study in the oligotrophic Mediterranean Sea. Biogeosciences **11**: 5607–5619. doi:10.5194/bg-11-5607-2014

Quast, C., and others. 2013. The SILVA ribosomal RNA gene database project: Improved data processing and web-based tools. Nucleic Acids Res. **41**: 590–596. doi:10.1093/nar/gks1219

R Core Team. 2016. R: A language and environment for statistical computing. R Foundation for Statistical Computing.

Rahav, E., and others. 2016. Evaluating the impact of atmospheric depositions on springtime dinitrogen fixation in the Cretan Sea (Eastern Mediterranean)—a mesocosm approach. Front. Mar. Sci. **3**. doi:10.3389/fmars.2016.00180

Ridame, C., J. Dekaezemacker, C. Guieu, S. Bonnet, S. L'Helguen, and F. Malien. 2014. Phytoplanktonic response to contrasted Saharan dust deposition events during mesocosm experiments in LNLC environment. Biogeosci. Discuss. **11**: 4783–4800. doi:10.5194/bg-11-4783-2014

Saito, M. A., and D. L. Schneider. 2006. Examination of precipitation chemistry and improvements in precision using the $Mg(OH)_2$ preconcentration inductively coupled plasma mass spectrometry (ICP-MS) method for high-throughput analysis of open-ocean Fe and Mn in seawater. Anal. Chim. Acta **565**: 222–233. doi:10.1016/j.aca.2006.02.028

Schloss, P. D., and others. 2009. Introducing mothur: Open-source, platform-independent, community-supported software for describing and comparing microbial communities. Appl. Environ. Microbiol. **75**: 7537–7541. doi:10.1128/AEM.01541-09

Stein, A. F., R. R. Draxler, G. D. Rolph, B. J. B. Stunder, M. D. Cohen, and F. Ngan. 2015. NOAA's HYSPLIT atmospheric transport and dispersion modeling system. Bull. Am. Meteorol. Soc. **96**: 2059–2077. doi:10.1175/BAMS-D-14-00110.1

Takemura, A. F., D. M. Chien, and M. F. Polz. 2014. Associations and dynamics of Vibrionaceae in the environment, from the genus to the population level. Front. Microbiol. **5**: 38. doi:10.3389/fmicb.2014.00038

Tinker, K. A., and E. A. Ottesen. 2016. The core gut microbiome of the American cockroach, *Periplaneta americana*, is stable and resilient to dietary shifts. Appl. Environ. Microbiol. **82**: 6603–6610. doi:10.1128/AEM.01837-16

Tsiaras, K. P., S. Christodoulaki, G. Petihakis, C. Frangoulis, and G. Triantafyllou. 2017. Model simulations of a mesocosm experiment investigating the response of a low nutrient low chlorophyll (LNLC) marine ecosystem to atmospheric deposition events. Front. Mar. Sci. **4**: 120. doi:10.3389/fmars.2017.00120

Wang, Q., G. M. Garrity, J. M. Tiedje, and J. R. Cole. 2007. Naïve Bayesian classifier for rapid assignment of rRNA sequences into the new bacterial taxonomy. Appl. Environ. Microbiol. **73**: 5261–5267. doi:10.1128/AEM.00062-07

Westphal, D. L., C. A. Curtis, M. Liu, and A. L. Walker. 2009. Operational aerosol and dust storm forecasting. IOP Conf. Ser. Earth Environ. Sci. **7**: 012007. doi:10.1088/1755-1307/7/1/012007

Westrich, J. R., and others. 2016. Saharan dust nutrients promote *Vibrio* bloom formation in marine surface waters. Proc. Natl. Acad. Sci. USA **113**: 5964–5969. doi:10.1073/pnas.1518080113

Westrich, J. R., D. W. Griffin, D. L. Westphal, and E. K. Lipp. 2018. *Vibrio* population dynamics in mid-Atlantic surface waters during Saharan dust events. Front. Mar. Sci. **5**: 12. doi:10.1073/pnas.1518080113

Wuttig, K., and others. 2013. Impacts of dust deposition on dissolved trace metal concentrations (Mn, Al and Fe) during a mesocosm experiment. Biogeosciences **10**: 2583–2600. doi:10.5194/bg-10-2583-2013

Zhang, R., and others. 2019. Growth of marine *Vibrio* in oligotrophic environments is not stimulated by the addition of inorganic iron. Earth Planet. Sci. Lett. **516**: 148–155. doi:10.1016/j.epsl.2019.04.002

Acknowledgments

This work was supported by NSF Biological Oceanography award OCE 1357423 (TB, JRW, EKL, and EAO), OCE 1357154 (MSW), and OCE 1357140 (AME and WML). Dr. Xian's work is supported by the Office of Naval Research, Code 322. Stage IV precipitation data provided by NCAR/EOL under the sponsorship of the National Science Foundation, https://data.eol.ucar.edu/.

Conflict of Interest

None declared.

Submitted 18 September 2018
Revised 29 May 2019
Accepted 04 July 2019

Associate editor: Anya Waite